Intelligent Remote Sensing Scene Classification Model for On-Board Training of Resource-Constrained Devices

Ahmad Khaldi[1,*], Josef Al Jumayel[2]

[1]Mutah University, Faculty of Science, Jordan

[2]Faculty Of Science, Beirut Arab University, Beirut, Lebanon

Emails: khaldiahmad1221@gmail.com; Josefjumayel113@gmail.com

Abstract

Remote Sensing Scene Classification (RSSC) is the distinctive classification of remote sensing images into numerous classes of scene classifications based on the image content. RSSC plays a significant role in several domains, like land mapping, agriculture, and the classification of disaster-prone regions. The Internet of Things (IoT) is a dynamic global network of devices, for example, vehicles, sensors, actuators, surveillance cameras, etc. These interconnected objects were distinctively recognizable and they could separately transfer and obtain valuable data through the network. However, satellite images were frequently degraded and blurred owing to aerosol dispersion under haze, fog, and other weather circumstances, decreasing the color fidelity and contrast of the image. To use effectual RSSC in real-time, widespread researchers concentrate on creating aerospace image processing systems, like airborne or spaceborne systems. Recently, with the quick improvement of deep learning (DL) and Machine learning (ML) techniques, the performance of RSSC has significantly developed owing to the hierarchical feature representation learning. Both technique has greater achievement in the domain of image scene classification. This study presents a Leveraging Tiny Convolutional Neural Networks with a Water Cycle Algorithm for Remote Sensing Scene Classification (LTCNN-WCRSSC) model. The LTCNN-WCRSSC technique is designed for efficient RSS classification in resource-constrained devices with on-board training capabilities. At first, the LTCNN-WCRSSC model applies image processing using a median filter (MF) to eliminate the noise. Next, the feature extraction process can be exploited by the ConvNeXt-Tiny method. For the RSSC model, the spatiotemporal attention bidirectional long short-term memory (STA-BiLSTM) technique is performed. Eventually, the water cycle algorithm (WCA)-based hyperparameter choice process can be performed to optimize the classification results of the STA-BiLSTM algorithm. The experimental evaluation of the LTCNN-WCRSSC technique takes place using a benchmark image dataset. The stimulated results indicated the superior performances of the LTCNN-WCRSSC model over other approaches.

Keywords: ConvNeXt-Tiny; Remote Sensing Scene Classification; Water Cycle Algorithm; Resource-Constrained Devices; Image Preprocessing

1. Introduction

Nowadays, people are observing fast growth in almost every field of life due to the rising tendencies of communication and collaborative technology [1]. The fast development, integration, and deployment of robotics, IoT, drones, artificial intelligence (AI), edge or cloud computing, future communication networks, aerial access networks, and big data analytics have also been accepted as important enablers for several smart city applications [2]. Owing to aerial access networks that are recognized based on both lower and higher altitude platforms, after being incorporated with satellite, physical, and IoT infrastructures, allow a comprehensive access network with global coverage and different quality-of-service provisions [3]. In recent times, developments in progressive aerial technologies and devices, like satellites, the growth of small, smart, and economical communication networks, and the larger availabilities of unmanned vehicles and aerial drones, have converted many surveillance and

Doi: https://doi.org/10.54216/JCHCI.090101
Received: October 19, 2024 Revised: December 05, 2024 Accepted: January 10, 2025

security applications. Additionally, after being connected to satellites and future communication networks, these devices furthermore improve real-time assistance for smart cities [4].

Recently, as remote sensing imaging (RSI) technology has grown, the resolution of RSI remains getting higher and higher, and the RSI application is broadly concerned. RSI comprises rich texture features and scene semantic information, which are of huge application value in agriculture production, national defense security, disaster warning, and so forth. RSSC technologies are of greater significance to the understanding and interpretation of RSI and are a critical investigation branch in RSI processing [5]. Nevertheless, the RSSC model still faces the next dual challenges. Regarding algorithm accuracy, the features of RSI with numerous scene types and higher similarities between groups, make the RSSC challenging [6]. Concerning algorithm efficacy, after challenging huge remote sensing data, computing equipment is required to implement intelligent, real-time, and large-scale calculations. The higher complexities of the methods depend on higher-performance computing devices, leading to important computation prices. Hence, it's mainly significant for considering the accuracy and computational efficacy of the classification model in the RSSC analysis [7].

Over the past few years, deep learning (DL) has drawn attention in the RS communities due to its superior execution in comparison with traditional models [8]. DL has been stimulated by the biological brain and utilizes easy but extremely interrelated units to imitate cerebral mechanisms. Besides spatial and spectral features, DL has an enormous probability of exploiting semantic data from input images. Convolutional neural networks (CNNs) that represent the utmost familiar DL algorithm for image identification tasks are applied in different available manuscripts in the RS field, by advanced outcomes [9]. Nevertheless, the majority of the said work used extremely higher-resolution satellite and aerial imagery for CNN training. Based on a review investigation only a limited investigation has accepted low- or medium-resolution RS data for image segmentation or scene classification tasks. The acceptable performance of the lightweight method regarding stability, speed, and accuracy offers technical and theoretical support for the execution of effective RSSC [10].

This study presents a Leveraging Tiny Convolutional Neural Networks with a Water Cycle Algorithm for Remote Sensing Scene Classification (LTCNN-WCRSSC) model. The LTCNN-WCRSSC technique is designed for efficient RSS classification in resource-constrained devices with on-board training capabilities. At first, the LTCNN-WCRSSC model applies image processing using a median filter (MF) to eliminate the noise. Next, the feature extraction process can be exploited by the ConvNeXt-Tiny method. For the RSSC model, the spatiotemporal attention bidirectional long short-term memory (STA-BiLSTM) technique is performed. Eventually, the water cycle algorithm (WCA)-based hyperparameter choice process can be performed to optimize the classification results of the STA-BiLSTM technique. The experimental evaluation of the LTCNN-WCRSSC technique takes place using benchmark image datasets.

2. Related Works

Wu et al. [11] introduce a target-aware knowledge distillation (TAKD) technique for RSSC. By studying the features between the background and target areas of the RS images, the TAKD could adaptably extract the knowledge from the trainer method to produce a lightweight student method. In particular, the author initially proposes a target-extracting module, which uses heatmaps to highlight targeted areas on the teacher's feature maps. Le et al. [12] proposed recognizing the utmost effectual pre-trained models for the identification of land use in onboard satellite processing, highlighting attaining great precision, computing efficacy, and strength against noisy data circumstances usually faced in satellite-based inference. Rashid et al. [13] present a TinyVQA, a new multi-modal deep neural network (DNNs) for graphical question-responding tasks, which is used on the source-restrained tiny ML hardware. TinyVQA utilizes a supervised attention-based method to study in what way to respond to problems regarding images utilizing either language or vision conditions. Wang et al. [14] presented a new change detection (CD) based on the knowledge distilling (CDKD) technique, which syndicates channel-spatial-normalized (CSN) distillations and prototypic contrastive distillations. PC distillation characterizes the distribution of features by computing the variances among the pixel characteristics comparisons and their negative and positive patterns and enhances the student model recognition capability in altered areas, which have equivalent features to the contextual by imitating the related feature distribution.

Shendy and Nalepa [15] propose these challenges by exploiting a fusion of model- and data-centric techniques to create a generalizing still effectual and source-frugal DL methods for multi-class satellite image identification in the few-shot learning environments. This combined approach can be expressed to improve classifier performances while considering the distinctive demand of an image study chain onboard OPS-SAT, a nanosatellite directed by the European Space Agency. Dai et al. [16] present an effectual RSSC technique called a multi-scale dense remaining connection system. The technique can be separated into 3 parts. Initially, multi-stream feature extraction modules are proposed that efficiently use features on dissimilar measures for extracting various levels

Doi: https://doi.org/10.54216/JCHCI.090101
Received: October 19, 2024 Revised: December 05, 2024 Accepted: January 10, 2025

of data. Next, the dense remaining connected feature fusion (FF) technique can be presented that enables an extensive choice of FF. The Correlation Attention Module study features representations on various levels.

Ye et al. [17] present a novel progressive learning system, called effectual channel attention-based multiscale depth-wise network (ECA-MSDWNet), in which ECA enhances the model capability to concentrate on crucial data in difficult situations, and MSDW Conv extracts multiscale features in a fine-grained manner. Additionally, in the progressive learning method, the author develops novel components based on a dynamic-structure technique to fit the residues among the old model outputs and labels, improving the novel method's flexibility for novel tasks while preserving the performances of the previous tasks. Liu et al. [18] present an effectual method structure, the self-correction feature enhancement fusion network (SCECNet), intended to enhance scene image handling abilities. Primarily, feature pyramid networks (FPNs) based on ResNet-50 can be used as the backbones for feature extraction that aids mitigate feature loss for insignificant targets. Next, a new lightweight channel attention mechanism has been intended to decrease the variances among the features from various layers while restraining inappropriate data.

3. Materials and Methodology

In this work, we have intended and developed a LTCNN-WCRSSC algorithm. The LTCNN-WCRSSC technique is designed for efficient RSS classification in resource-constrained devices with on-board training capabilities. To accomplish that, the LTCNN-WCRSSC model contains various phases like feature extraction, image preprocessing, classification model, and hyperparameter tuning method. Fig. 1 signifies the working of the LTCNN-WCRSSC model.

3.1. Image Preprocessing using MF

At first, the LTCNN-WCRSSC model applies image preprocessing using MF to eliminate the noise. The ML is a critical method in RSSC, mainly for on-board training of resource-constrained devices [19]. By efficiently decreasing noise in maintaining edges, the median filter improves the input data quality, enabling more precise scene analysis. Its computing efficacy makes it suitable for devices with restricted processing power, assuring that important features are taken without overpowering system sources. This pre-processing stage helps in enhancing the strength of ML methods, enabling real-time study in active surroundings. As an outcome, it aids effectual data classification and acquisition, vital for applications in urban planning, agriculture, and forestry. Generally, incorporating median filtering into remote sensing workflows enhances performance while preserving operative possibility.

Doi: https://doi.org/10.54216/JCHCI.090101
Received: October 19, 2024 Revised: December 05, 2024 Accepted: January 10, 2025

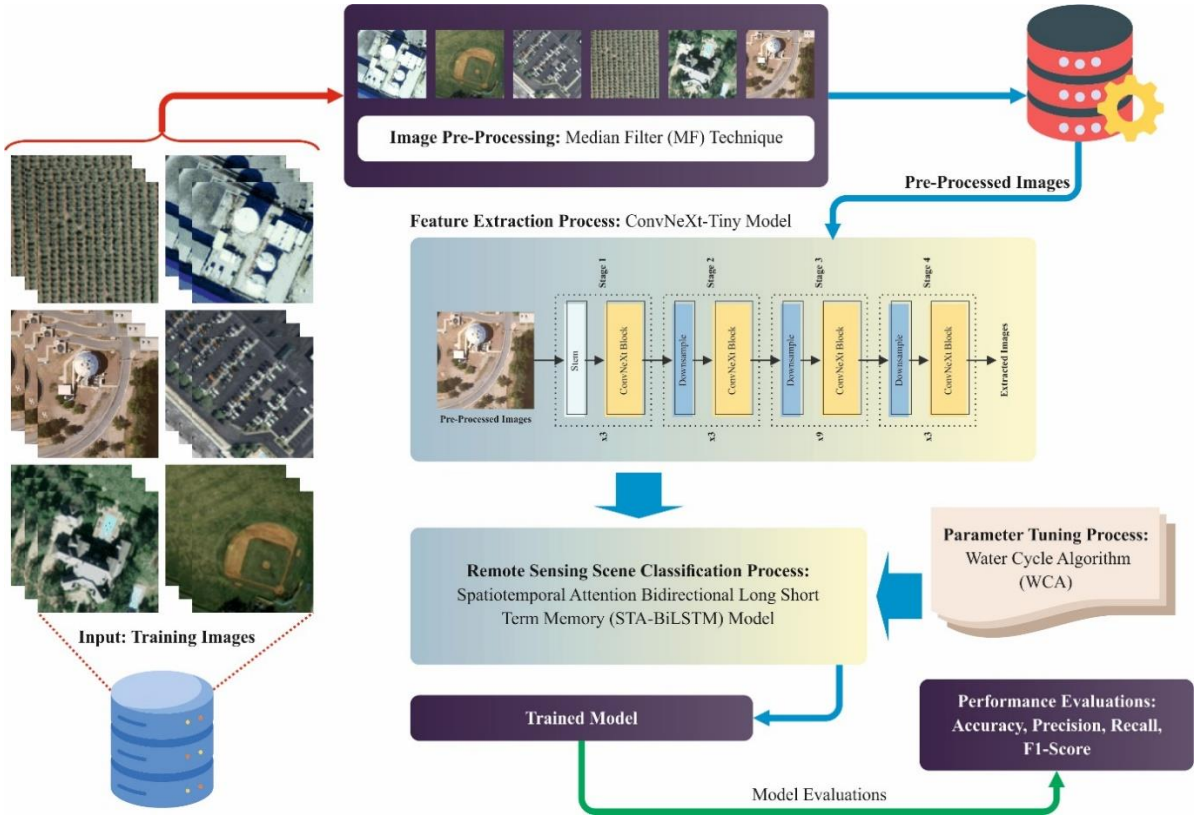

Figure 1: Overall Workflow of the LTCNN-WCRSSC model

3.2. ConvNeXt-Tiny-based Feature Extraction Process

Then, the process of feature extraction can be used by the ConvNeXt-Tiny model. The Conv Next-Tiny method utilizes understands the structure blocks, which contain depth-wise convolutional layers with kernel sizes of 7 x 7 and n channels that equal the input feature channel; layer normalization (LN); 1 x 1 convolutional layer with various channels equivalent to 4, activate with GELU; 1 x 1 convolutional layer accompanied by various channels equivalent to n. The results of this method are going to be computed selectively with the original input features [20].

The complete ConvNext-Tiny structure contains 4 phases: the 1st phase contains three ConvNeXt block cycles, the 2nd phase of three cycles, the 3rd phase of nine cycles, and the 4th phase of three cycles. At the start of every phase before penetrating the ConvNext block, a down-sampling method can be included that decreases the input feature width and length to double and half the amount of channels. The endeavor to develop the common ResNet method into ConvNext isn't restricted to changing its structure, but also enhancing the training method by utilizing AdamW optimizer. Researchers also utilize a few data augmenting methods over usual methods like RandAugment, MixUp, and CutMix. Label Smoothing regularization (LSR) and Stochastic Depth methods are also combined, inducing inexpensive performances on typical image identification tasks (ImageNet). For this study, we will utilize the ConvNext-Tiny method by pretrained weight.

The Attention Mechanism improvement can be based on human habits/characteristics while seeing information, particularly in the image background. While seeing information, humans will typically concentrate on seeing the significant parts, like dividing the focal point from the contextual. Attention Mechanism can be very beneficial for object detection and classification difficulties since it could validate the features, which are significant in these backgrounds by analyzing the image.

The initial work on Channel Attention is the Squeeze-and-Excitation Network (SE-Net). Though the SE-Net structure can be much easier, including it to current CNN achieved the ImageNet contest. Essentially, SE-Net contains dual consecutive Fully Connected (Dense or FC) through dual kinds of activation function, ReLU into the initial FC and sigmoid within the next FC. The inputs for the block FC can be Global Average Pooling (GAP)

Doi: https://doi.org/10.54216/JCHCI.090101
Received: October 19, 2024 Revised: December 05, 2024 Accepted: January 10, 2025

depending on the feature map channel. Later, the block FC operating outcome can be channel-based multiplied across the primary feature maps. The concluding outcome of SE-Net is measured as the significance weights for every channel.

ECANet is an attention mechanism structure, which is an alteration of SE-Net. Research scholars contend that the drawback of SE-Net is the dimensionality reduction method afterward GAP, while decreasing difficulty, deletes corresponding relationships or information among channels. In this work, they develop a method that contains a distinctive FC layer afterward GAP called SE-Var3, thus it studies the similarity among individual channels and each and every other channel. This method created greater Top-5 and Top-l precision than vanilla SE-Net. SE-Var3 has been additionally changed to decrease its difficulty by not studying the equivalence of individual channels to each and every other channel, but simply to the k adjacent channels. This process is simply performed utilizing the one-dimension convolutions. Then, the outcomes of the $1D$ convolutions are stimulated utilizing sigmoid and were multiplied elementwise by the primary feature map X.

The computation of ECANet is stated in Eq. (1).

$$F_{ECA}(x) = \sigma\left(Conv1D_k\left(GAP(x)\right)\right) \otimes x \tag{1}$$

The following question is how to identify the optimum values of k. Now they offer Eq.(2) that can be expressed depending on the statement, which the amount of channel C or tensor dimension input to the GAP can be frequently a strength of 2. In the meantime, the values of the b and γ were attained by experimentations ($b = 1$ and $\gamma = 2$). ECANet gives higher precision than CBAM and SE-Net and has a lesser difficulty and amount of parameters.

$$k = \psi(C) = \left|\frac{\log_2(C)}{\gamma} + \frac{b}{\gamma}\right|_{odd} \tag{2}$$

Essentially, we establish the module of ECANet in the current backbones of CNN, and in the training, the weightings of the $Conv1D_k$ Layer can be studied. The weight $Conv1D_k$ signifies the significance grade of every adjacent channel. Hereby, we can direct the backbone network to provide additional attention to higher-significance channels.

LSR is a technique used in ML, especially in the task of classification, to improve the generalization method as well as alleviate overfitting. During the typical set-up, wherever the model predicts possibilities for every class, label smooth differs by allocating a smaller possibility to improper class in training. This technique has been initially proposed in the study on Inception structure, and the notion of utilizing LSR for RSSC tasks has been stimulated.

The key notion behind the LSR is never to create the method too confidently due to the one-hot encoding of the input. Like this, the crisp encoder will neglect each other class (that isn't the targeted model classes) in the cross-entropy loss function computation. In the meantime, in the RSSC case, a scene image possibly contains various objects of dissimilar classes, whereas the classes of the utmost leading object become image-assigned labels. LSR will relabel the input encoding with Eq. (3).

$$y_i = \begin{cases} 1 - \varepsilon; i = c \\ \dfrac{\varepsilon}{k-1}; i \neq c \end{cases} \tag{3}$$

i represents the amount of class, y_i signifies the class ground-truth label i, c means the targeted class, k presents the overall amount of classes, and ε signifies the factors of smoothing. We will utilize $\varepsilon = 0.1$ during this experimentation. This equation assigns a tempered probability to either another class or the true class. The LSR addition can be anticipated to create a model much stronger and having anti-noise capability.

In this experimentation, ECANet can be combined after every phase of ConvNext-Tiny. The incorporation of ECANet afterward the ConvNeXt-Tiny phase improves the feature and eliminates redundant or tedious data. The study discusses that consideration of the spatial and or channel aspects afterward every phase can be significant because the width and length of the features after the phase were decreased to half of the creation of the phase, and the amount of channels was multiplied. Weighting every channel and or feature spatial location will improve the features much more efficiently therefore the following phase of ConvNeXt could study superior input features.

3.3. STA-BiLSTM based Classification Model

Doi: https://doi.org/10.54216/JCHCI.090101
Received: October 19, 2024 Revised: December 05, 2024 Accepted: January 10, 2025

For the RSSC model, the LTCNN-WCRSSC algorithm employs the STA-BiLSTM technique. The network of LSTM contains of gate and memory cell to the conventional recurrent neural networks (RNNs) [21]. Cell (c) is employed to note states of neurons that are attained by a point-wise and sigmoid multiplication process. This execution particularly permits data to permit over the gate. The LSTM can be intended with dual gates for controlling the quantity of data within the memory cell state ($Cell$): The forget gate is taken as the memory gap that defines how much-preceding cell state memory can recollect till the present moment. The input gate determines how much novel input information must be included in the state of a cell at the present moment, beside the candidate gates. The candidate gate handles the fusion ratio among the past data and present stimulation, therefore defining the volume of the novel cell state to be upgraded. Lastly, an output gate manages several data that can be output from the states of the cell, certifying that only the most vital data is carried. LSTM can capture long-dependency data in input over the structure of the gate which lightens the issues of gradient explosion and vanishing.

The forget gate is demonstrated in Eq. (4), as below:

$$f_i = \sigma\left(W_f^T \times s_{t-1} + U_f^T \times x_t + b_f\right) \tag{4}$$

The input gate is shown in Eq. (5):

$$i_r = \sigma(W_i^T \times s_{t-1} + U_i^T \times x_t + b_i) \tag{5}$$

The mathematical equation of the candidate gate can be expressed in Eq. (6):

$$C_t' = \tanh(W_c^T \times s_{t-1} + U_c^T \times x_t + b_c) \tag{6}$$

The formulation of the memory cell is presented in Eq. (7), as below:

$$C_t = f_t \times C_{t-1} + i_t \times C_t' \tag{7}$$

The output gate is displayed in the Eq. (8):

$$O_t = \sigma(W_o^T \times s_{t-1} + U_o^T \times x_t + b_o) \tag{8}$$

The concluding output is presented in Eq. (9):

$$s_t = O_t \times \tanh(C) \tag{9}$$

The loss function formulation is expressed in Eq. (10):

$$\min J(\theta) = \sum_{t=1}^{T} loss\left(y^{(t)} \wedge, y^{(t)}\right) \tag{10}$$

In conventional time-series processing, LSTM usually only uses past information and disregards future data. The Bi-LSTM utilizes dual separate hidden layers (HLs) that depend upon LSTM to procedure the sequential data in both the directions of backward and forward, links the dual HLs to the similar layer of output, and keeps both latter and previous data as the present-time on the time-series data. So ideally, the performances will be superior to the unidirectional LSTM. Bi-LSTM HL output contains an activation output of both backward and forward HL. This mechanism shows how data from both directions are combined and together concerns the layer of output, delivering a deeper perception and improved capability for time-series data. Bi-LSTM is not capable of capturing the dissimilar impacts of diverse input features and time points to the final price. It is highly enhanced for classical techniques by computing the attention probability distribution, emphasizing the portion of a vital input on output, and permitting the computation sources to major tasks with restricted power of computational. In this situation, an original spatiotemporal attention mechanism is specially intended to take the dynamic spatiotemporal correlations, which unites both attention of temporal and spatial to more precisely recognize and use the data that is most vital for prediction.

In the dimension of spatiality, the interaction among dissimilar input features is extremely dynamic. Due to this cause, a spatial attention mechanism is employed to selectively take the adaptive correlation among nodes into the spatial dimensions. It extends the effect of every exterior feature on the final value by demonstrating the attention weight, which aggregates to one. For every timestep, t, the weight is employed to evaluate several attention the node must concentrate on other nodes for calculating the prospect closing price. While Bi-LSTM

Doi: https://doi.org/10.54216/JCHCI.090101
Received: October 19, 2024 Revised: December 05, 2024 Accepted: January 10, 2025

cell can uphold long-term dependency by keeping temporal data over the cell and handling the upsurge or reduction in information over a gate mechanism, the time-based data measured over gates affects the Bi-LSTM to alter its cell states in every time window T, a last state inclines to recollect data regarding the utmost current input when equated to the past input. In the longer perspectives, the regular method might undervalue an effect of previous states.

The temporal attention mechanism can be employed to know the impact of the hidden state (HL) in every time window. While the attention mechanism is employed, the Bi-LSTM cells keep temporal data to evaluate the significance of these dissimilar cell states. Spatial correlations were signified by the attention mechanisms of spatial that allocate attention weight to original features. Then, the temporal relevance is recognized over the temporal attention mechanism by allocating attention weight to the HL. The spatiotemporal attention mechanism unites both the temporal and spatial correlations, letting the neural networks routinely concentrate more attention on effective information. Fig. 2 depicts the architecture of the STA-BiLSTM method.

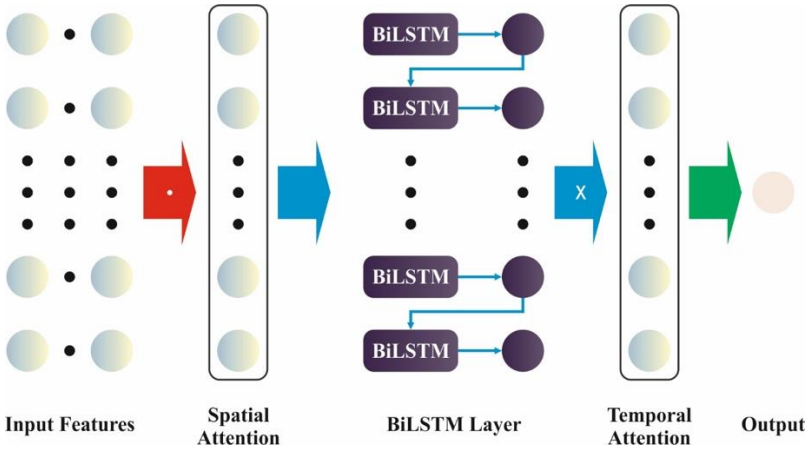

Figure 2: Structure of STA-BiLSTM model

3.4. WCA-based Hyperparameter Tuning Method

Eventually, the WCA-based hyperparameter choice process is performed to improve the classification outcomes of the STA-BiLSTM system. Corresponding to previous meta-heuristic models, the proposed algorithm initiates with an early population named the raindrops [22]. Primarily, we assume rainfall like precipitation is present. Similar to a sea, the ideal person becomes nominated to be the finest raindrop. Afterward, various unexpected drops are considered rivers, along with residue rainfalls are labeled stream which flow in the ocean and the rivers. The clarification of all river flowing rates which state the quantity of water it obtains from the stream is discovered in the subsequent subcategories.

Initialization

To resolve an optimization difficulty using population-based meta-heuristic algorithms, the problem variables' values are required to be collected into a group. This kind of arrays can be devoted to the chromosomes in GA terms and as a particle location in PSO terms. As a solitary solution, this can be the cause for the recommended model named Raindrop. It is a single array in a dimension optimization issue. This represents the description from it array:

$$Raindrop = [r_1, r_2, \dots, r_N] \tag{11}$$

A candidate describing a raindrop matrix of dimension N_{pop}, N_{var} has been built to start the optimization model (for example raindrop population). Te randomly formed matrix W, so, is as demonstrated (rows mean the population variable counts, and column the design variable counts, correspondingly):

Doi: https://doi.org/10.54216/JCHCI.090101
Received: October 19, 2024 Revised: December 05, 2024 Accepted: January 10, 2025

$$Population\ of\ Raindrop = \begin{bmatrix} r_1^1 & r_2^1 & r_3^1 & \dots & r_{Nvar}^1 \\ r_1^2 & r_2^1 & r_3^1 & \dots & r_{Nvar}^1 \\ r_1^2 & r_2^1 & r_3^1 & \dots & r_{Nvar}^1 \\ . & . & . & \dots & . \\ . & . & . & \dots & . \\ . & . & . & \dots & . \\ r_1^2 & r_2^1 & r_3^1 & \dots & r_{Nvar}^1 \end{bmatrix} \quad (12)$$

The values of every decision variable, $[r_1, r_2, \dots, r_{Nvar}]$ are signified as a pre-determined set for different issues or as a floating points amount (real values) for constant difficulties. The cost function valuation (X) that can be offered in the following, produces the raindrop cost.

$$X_i = f\left(r_1^i, r_2^i, \dots, r_{Nvar}^i\right), i = 1,2, \dots, Npop, \quad (13)$$

Here N_{pop} and N_{var} refer to the early population (raindrop counts) and the design variable counts, correspondingly. N_{pop} raindrops are produced in the early phase. Several U_{sr} from the best persons (minimal values) were selected as sea as well as the rivers. A raindrop has been observed as a sea if its value represents lowermost of every other. U_{sr} stands for the overall unique sea as stated in Eq. (14) along with river counts that were a user parameter in Eq. (15) is applied to calculate the residue from the population that contains raindrops, which make streams, which flow to the river or might run directly towards the sea.

$$U_{sr} = number\ of\ rivers\ + 1\ (sea), \quad (14)$$

$$Y_{raindrop} = Npop - U_{sr}. \quad (15)$$

Now is the formula, which is utilized to assign raindrops to the rivers as well as the sea depending on flowing strength:

$$YS_n = round\left\{\left|\frac{X_i}{\sum_{i=1}^{U_{sr}} X_i}\right| \times y_{raindrops}\right\}, n = 1,2,3, \dots, U_{sr}, \quad (16)$$

Now, YS_n is how many streams flow into a known water body or river. The streams were made in the raindrops and combined to make them novel rivers, as specified in the Initial theory segment. It is also likely for particular streams to drain into the sea. The ocean is the final, last end for each and every stream and river. The stream schema aspect is running near a specific river. Over their connection lines, a stream runs to the river at a distance, which can be randomly selected and presented as demonstrated:

$$Z \in (0, C \times D), C > 1, \quad (17)$$

Now C denotes a value near to two that drops between one and two. One can choose two for the best values for C. The symbol due to the present distance between the stream and the river is D. A number distributed at random among zero and $(C \times D)$, distributed both consistently and based on some appropriate distribution has been characterized through the values of Z in Eq. (17). Streams may flow near rivers in different directions if the values of A surpasses unity. Rivers that run into the ocean also enable believed off with this concept. Therefore, the subsequent can be the novel location for streams and rivers:

$$Z_{stream}^{i+1} = Z_{stream}^i + rnd \times C \times \left(Z_{river}^i - Z_{stream}^i\right), \quad (18)$$

$$Z_{river}^{i+1} = Z_{river}^i + rnd \times C \times \left(Z_{sea}^i - Z_{river}^i\right), \quad (19)$$

In which the randomly generated number between $zero$ and one, rnd is distributed uniformly. Rivers and Streams change locations when the solution they offer balances that of the linked rivers (streams turn out to be rivers and rivers turn into streams). In the same way, the sea and rivers can substitution like this method. An exchange between the river and a stream that represents an ideal selection.

Evaporation condition

A main aspect that can prevent the model from meeting quickly is not fully formed evaporation or convergence. This can be proven by nature, whereas water can be out into the air by plants over photosynthesis and vaporizes in lakes as well as rivers. If water vaporizes, clouds take this up in the air, whereas it reduces in the cooler air and

Doi: https://doi.org/10.54216/JCHCI.090101
Received: October 19, 2024 Revised: December 05, 2024 Accepted: January 10, 2025

rains back off to the earth. Rain makes novel streams, which ultimately connect to rivers that drain into the sea. The circulation of water can be reviewed in the Initial idea section. The seawater in the proposed algorithm vaporizes as streams and rivers flow in the sea owing to the method of evaporation. The objective of presenting this theory is to avoid contracting local bests. The Pseudocode which follows determines how to determine whether a river drains in the sea.

$$If\left|Z_{sea}^{i} - Z_{river}^{i}\right| < \delta_{\max}, i = 1,2,3, U_{sr} - 1. \quad (20)$$

The process of rain and evaporation finishes whereas $\delta_{\max}$ refers to the small value that considers $zero$. Finally, a river has joined or reached the ocean when the distance between it and the sea can be less than $\delta_{\max}$. The process of evaporation has been applied in such a situation, and as is detected in nature, precipitation (rain) will start afterward with an adequate evaporation amount. In the locality of the sea, a bigger number for $\delta_{\max}$ rejects searching movement, while a smaller value upsurges it. Therefore, $\delta_{\max}$ controls the searching strength (the better choices) near the beach. The $\delta_{\max}$ value conformably declines as:

$$\delta_{\max}^{i+1} = \delta_{\max}^{i} - \frac{\delta_{\max}^{i}}{\max\_it} \quad (21)$$

Raining Process

The raining process has been applied after the process of evaporation is assured. As it rains, the new drops are divided into streams at numerous places (performing like mutation operators of GAs). The subsequent equation has been applied to identify the fresh places of the recently made streams:

$$Z_{stream}^{new} = Lb + rnd \times (Ub - Lb) \quad (22)$$

Whereas the presented problem describes the upper and lower limits, signified by ub and lb, correspondingly.

Once again, the best newly formed raindrop in comparison with a river, which drains in the sea. It is estimated that the residual rains will make novel streams, which flow straight to the ocean and rivers. To increase the computing efficiency and converging rates of the model for smaller issues, Eq. (23) is used simply for streams that end straight into the ocean. To improve near-sea exploration (the best answer) into the possible region for restricted challenges, this calculation searches for encouraging the formation of streams that run straight to the sea.

$$Z_{stream}^{new} = Z_{new} + \sqrt{\alpha} \times rnd(1, Nvar) \quad (23)$$

The WCA model improves a fitness function (FF) to get better classification performances. It identifies a positive integer to denote the superior performances of the candidate solutions. In this work, the reduction of the classification rate of error can be measured as the FF, as specified in Eq.(24).

$$fitness(x_i) = ClassifierErrorRate(x_i)$$

$$= \frac{number\ of\ misclassified\ samples}{Total\ number\ of\ samples} * 100 \quad (24)$$

4. Result Analysis

The performance evaluation of the LTCNN-WCRSSC model is verified under two datasets namely UC-Merced [23] and EuroSAT [24]. The UC-Merced dataset contains 2100 samples, each classes have a 100 samples such as Agricultural (L1), Airplane (L2), Baseball Diamond (L3), Beach (L4), Buildings (L5), Chaparral (L6), Dense Residential (L7), Forest (L8), Freeway (L9), Golf Course (L10), Harbor (L11), Intersection (L12), Medium Residential (L13), Mobile Home Park (L14), Overpass (L15), Parking Lot (L16), River (L17), Runway (L18), Sparse Residential (L19), Storage Tanks (L20), Tennis Court (L21). The EuroSAT dataset contains 1000 samples, each class holds 100 samples such as Annual Crop (L1), Forest (L2), Herbaceous (L3), Highway (L4), Industrial (L5), Pasture (L6), Permanent Crop (L7), Residential (L8), River (L9), Sea Lake (L10). Fig. 3 portrays the sample images.

Doi: https://doi.org/10.54216/JCHCI.090101
Received: October 19, 2024 Revised: December 05, 2024 Accepted: January 10, 2025

Figure 3: Sample images

Doi: https://doi.org/10.54216/JCHCI.090101
Received: October 19, 2024 Revised: December 05, 2024 Accepted: January 10, 2025

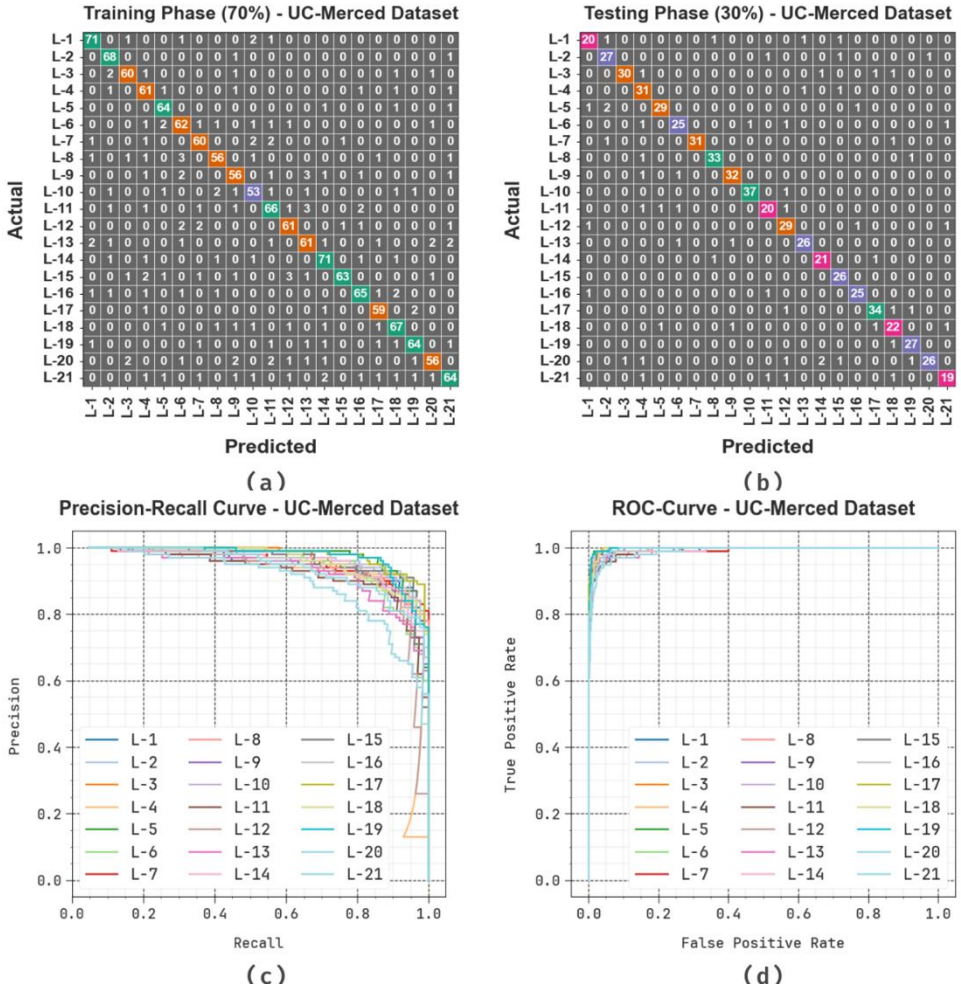

Figure 4: UC-Merced Dataset (a-b) Confusion matrices and (c) curve of PR and (d) curve of ROC

Fig. 4 represents the classification results of the LTCNN-WCRSSC model on the UC-Merced dataset. Figs. 4a-4b exhibits the confusion matrix with precise classification and recognition of all classes. Fig. 4c exhibits the PR analysis, representing greater performances across all class labels. Eventually, Fig. 4d shows the ROC analysis, signifying proficient results with greater ROC values for distinctive class labels.

In Table 1 and Fig. 5, the RSSC detection outcomes of the LTCNN-WCRSSC method can be denoted on the UC-Merced database. The outcomes stated that the LTCNN-WCRSSC algorithm appropriately differentiated all the samples. On 70%TRAPH, the LTCNN-WCRSSC system delivers an average $accu_y$ of 98.95%, $prec_n$ of 89.03%, $reca_l$ of 88.99%, and $F1_{score}$ of 88.96%. Moreover, on 30%TESPH, the LTCNN-WCRSSC methodology provides average $accu_y$ of 99.09%, $prec_n$ of 90.31%, $reca_l$ of 90.21%, and $F1_{score}$ of 90.13%.

Table 1: RSSC detection outcomes of LTCNN-WCRSSC technique on UC-Merced database

Class Labels	$Accu_y$	$Prec_n$	$Reca_l$	$F1_{score}$
70% TRAPH				
L-1	99.25	92.21	93.42	92.81
L-2	99.32	89.47	97.14	93.15
L-3	99.25	92.31	90.91	91.60
L-4	98.78	83.56	91.04	87.14
L-5	99.32	90.14	95.52	92.75
L-6	98.64	84.93	87.32	86.11
L-7	99.05	89.55	89.55	89.55
L-8	98.98	90.32	86.15	88.19

Doi: https://doi.org/10.54216/JCHCI.090101
Received: October 19, 2024 Revised: December 05, 2024 Accepted: January 10, 2025

L-9	98.64	84.85	84.85	84.85
L-10	98.78	85.48	85.48	85.48
L-11	98.64	86.84	86.84	86.84
L-12	98.98	88.41	89.71	89.05
L-13	98.57	85.92	84.72	85.31
L-14	98.98	88.75	92.21	90.45
L-15	99.12	96.92	85.14	90.65
L-16	98.98	90.28	89.04	89.66
L-17	99.32	90.77	93.65	92.19
L-18	98.91	88.16	90.54	89.33
L-19	99.12	92.75	88.89	90.78
L-20	98.84	90.32	83.58	86.82
L-21	98.50	87.67	83.12	85.33
Average	**98.95**	**89.03**	**88.99**	**88.96**
30% TESPH				
L-1	98.89	86.96	83.33	85.11
L-2	98.89	87.10	90.00	88.52
L-3	99.21	96.77	88.24	92.31
L-4	98.57	81.58	93.94	87.32
L-5	99.05	93.55	87.88	90.62
L-6	98.89	89.29	86.21	87.72
L-7	99.68	100.00	93.94	96.88
L-8	99.37	94.29	94.29	94.29
L-9	99.37	94.12	94.12	94.12
L-10	99.68	97.37	97.37	97.37
L-11	98.89	86.96	83.33	85.11
L-12	98.57	82.86	90.62	86.57
L-13	99.37	92.86	92.86	92.86
L-14	99.21	87.50	91.30	89.36
L-15	99.37	86.67	100.00	92.86
L-16	99.37	92.59	92.59	92.59
L-17	99.05	91.89	91.89	91.89
L-18	98.57	81.48	84.62	83.02
L-19	99.37	90.00	96.43	93.10
L-20	98.73	96.30	78.79	86.67
L-21	98.89	86.36	82.61	84.44
Average	**99.09**	**90.31**	**90.21**	**90.13**

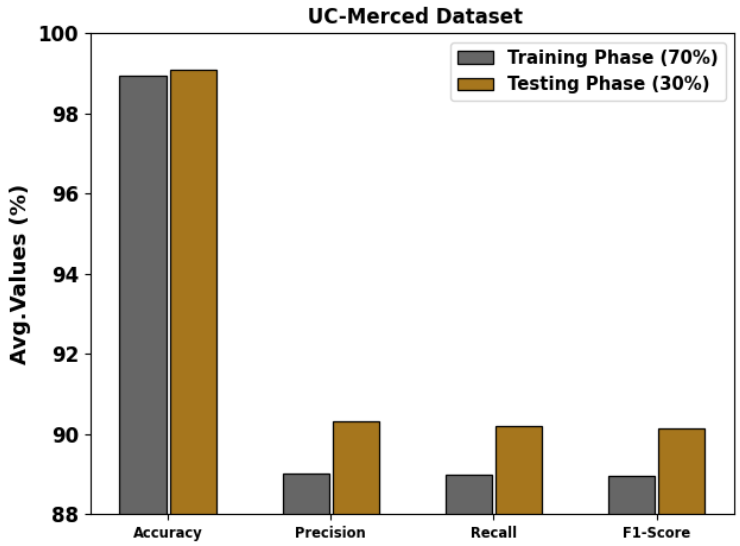

Figure 5: Average of LTCNN-WCRSSC technique on UC-Merced database

Doi: https://doi.org/10.54216/JCHCI.090101
Received: October 19, 2024 Revised: December 05, 2024 Accepted: January 10, 2025

In Fig. 6, the training $accu_y$(TRAAC) and validation $accu_y$(VLAAC) outcomes of the LTCNN-WCRSSC technique on the UC-Merced database can be displayed. The $accu_y$Values are estimated for 0-25 epoch counts. The figure emphasized that the TRAAC and VLAAC values display an increasing trend which reported the capability of the LTCNN-WCRSSC system with superior performance over various iterations. Furthermore, the TRAAC and VLAAC remain adjacent over the epochs, which specifies the least overfitting and exhibits boosted performances of the LTCNN-WCRSSC algorithm, promising constant prediction on hidden samples.

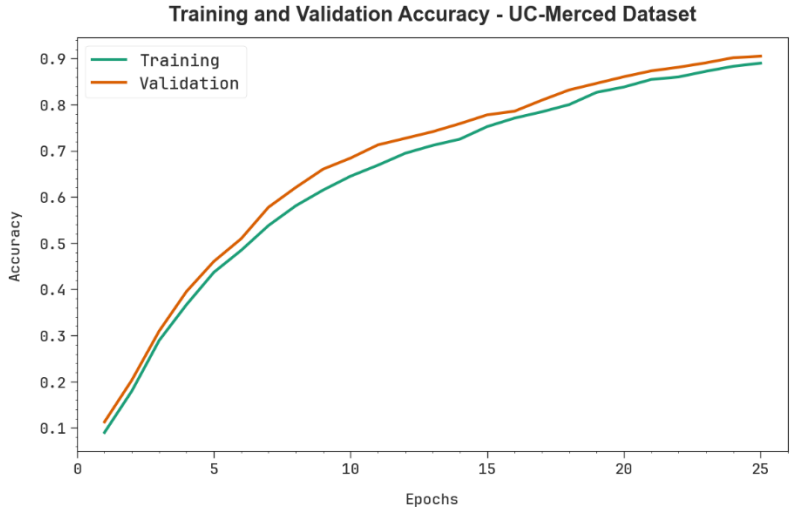

Figure 6: $Accu_y$ curve of LTCNN-WCRSSC model on UC-Merced database

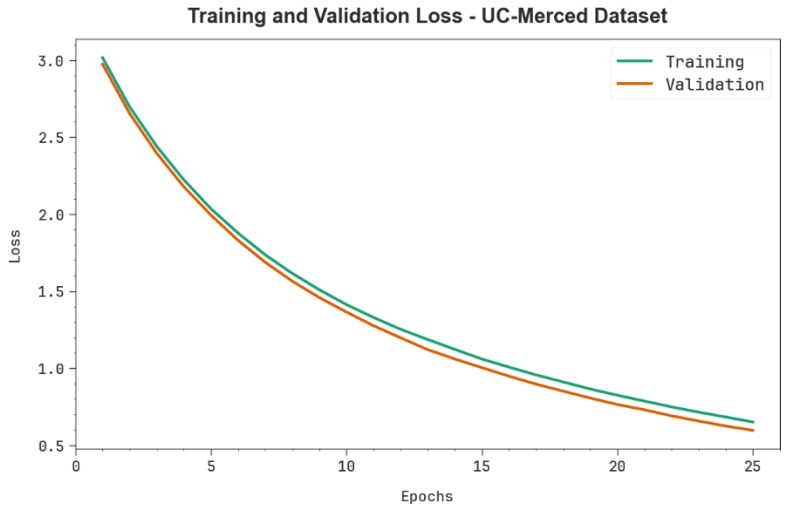

Figure 7: Loss curve of LTCNN-WCRSSC model on UC-Merced database

In Fig. 7, the TRA loss (TRALS) and VLA loss (VLALS) graph of the LTCNN-WCRSSC method on the UC-Merced database can be exhibited. The loss values are estimated for 0-25 epoch counts. It is denoted that the TRALS and VLALS values demonstrate a decreasing trend, notifying the ability of the LTCNN-WCRSSC technique to balance a trade-off between data fitting and generalization. The incessant reduction in loss values moreover promises the higher performances of the LTCNN-WCRSSC model and tunes the prediction results over time.

Fig. 8 represents the classification results of the LTCNN-WCRSSC model on the EuroSAT dataset. Figs. 8a-8b displays the confusion matrix with precise classification and recognition of all class labels. Fig. 8c exhibits the PR analysis, representing the highest performance across all class labels. Finally, Fig. 8d exhibits the ROC analysis, indicating proficient results with greater ROC values for different class labels.

Doi: https://doi.org/10.54216/JCHCI.090101
Received: October 19, 2024 Revised: December 05, 2024 Accepted: January 10, 2025

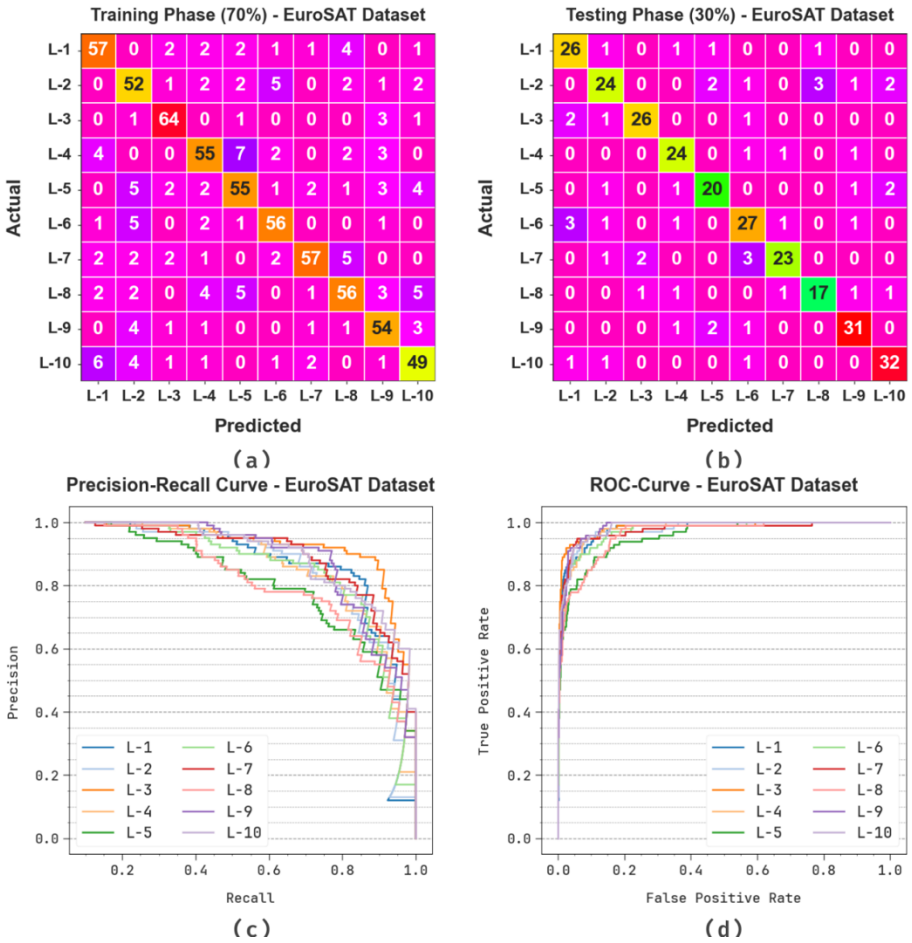

Figure 8: EuroSAT Dataset (a-b) Confusion matrices and (c) curve of PR and (d) curve of ROC

In Table 2 and Fig. 9, the RSSC recognition results of the LTCNN-WCRSSC technique can be signified on the EuroSAT dataset. The outcomes stated that the LTCNN-WCRSSC model appropriately distinguished all the samples. On 70%TRAPH, the LTCNN-WCRSSC system provides an average $accu_y$ of 95.86%, $prec_n$ of 79.40%, $reca_l$ of 79.45%, and $F1_{score}$ of 79.35%. Moreover, on 30%TESPH, the LTCNN-WCRSSC algorithm delivers an average $accu_y$ of 96.67%, $prec_n$ of 83.28%, $reca_l$ of 83.09%, and $F1_{score}$ of 83.11%.

Table 2: RSSC detection outcomes of LTCNN-WCRSSC technique on the EuroSAT dataset

Class Labels	$\boldsymbol{Accu_y}$	$\boldsymbol{Prec_n}$	$\boldsymbol{Reca_l}$	$\boldsymbol{F1_{score}}$
70% TRAPH				
L-1	96.00	79.17	81.43	80.28
L-2	94.57	69.33	77.61	73.24
L-3	97.86	87.67	91.43	89.51
L-4	95.29	78.57	75.34	76.92
L-5	94.57	75.34	73.33	74.32
L-6	96.86	82.35	84.85	83.58
L-7	97.00	89.06	80.28	84.44
L-8	94.71	78.87	71.79	75.17
L-9	96.29	78.26	83.08	80.60
L-10	95.43	75.38	75.38	75.38
Average	**95.86**	**79.40**	**79.45**	**79.35**

Doi: https://doi.org/10.54216/JCHCI.090101
Received: October 19, 2024 Revised: December 05, 2024 Accepted: January 10, 2025

30% TESPH				
L-1	96.67	81.25	86.67	83.87
L-2	95.00	80.00	72.73	76.19
L-3	97.67	89.66	86.67	88.14
L-4	97.33	82.76	88.89	85.71
L-5	96.67	80.00	80.00	80.00
L-6	95.00	77.14	79.41	78.26
L-7	97.00	88.46	79.31	83.64
L-8	97.00	80.95	77.27	79.07
L-9	97.00	86.11	88.57	87.32
L-10	97.33	86.49	91.43	88.89
Average	**96.67**	**83.28**	**83.09**	**83.11**

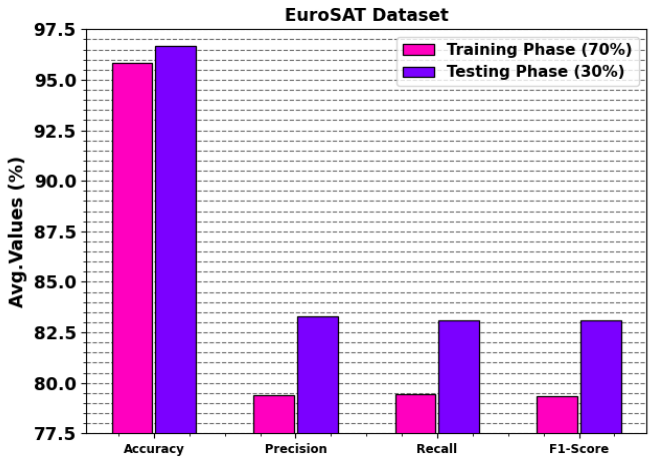

Fig. 9. Average of LTCNN-WCRSSC model on EuroSAT database

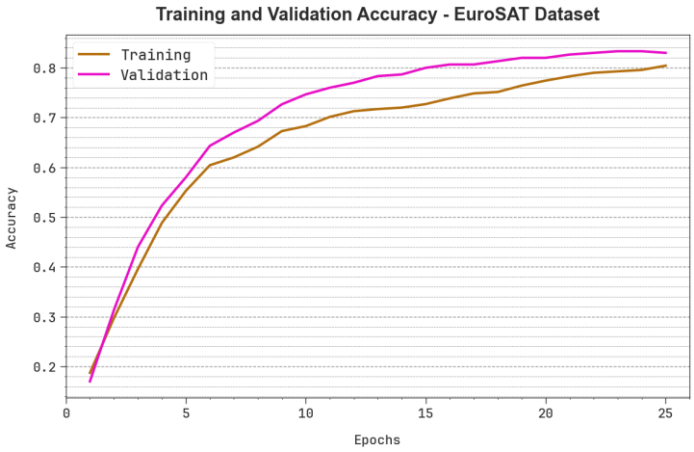

Figure 10: $Accu_y$ curve of the LTCNN-WCRSSC model on the EuroSAT database

In Fig. 10, the TRAAC and VLAAC outcomes of the LTCNN-WCRSSC technique on the EuroSAT dataset can be exhibited. The $accu_y$values are estimated for 0-25 epoch counts. The figure underlined that the TRAAC and VLAAC values display a growing trend which reported the capability of the LTCNN-WCRSSC system with superior performance over various iterations. Furthermore, the TRAAC and VLAAC remain adjacent over the

Doi: https://doi.org/10.54216/JCHCI.090101
Received: October 19, 2024 Revised: December 05, 2024 Accepted: January 10, 2025

epochs, which specifies the least overfitting and displays boosted performances of the LTCNN-WCRSSC algorithm, promising constant prediction on unnoticed samples.

In Fig. 11, the TRALS and VLALS graph of the LTCNN-WCRSSC method on the EuroSAT dataset can be shown. The loss values are estimated for 0-25 epoch counts. It is denoted that the TRALS and VLALS values demonstrate a reducing trend, reporting the capability of the LTCNN-WCRSSC methodology to balance a trade-off between generalization and data fitting. The incessant reduction in loss values furthermore promises greater performances of the LTCNN-WCRSSC technique and tunes the prediction outcomes over time.

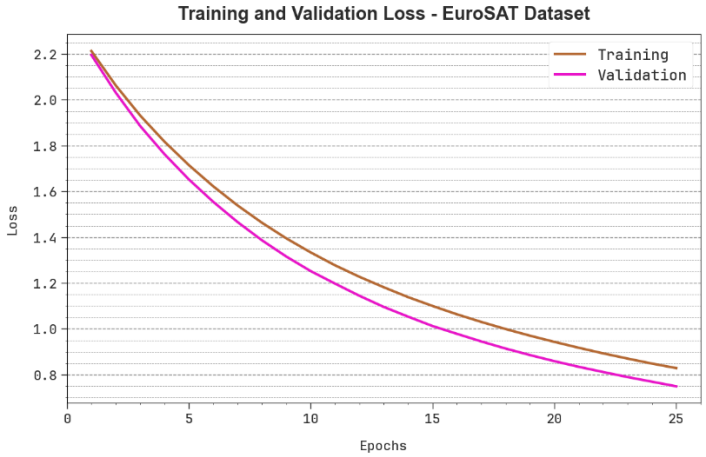

Figure 11: Loss curve of LTCNN-WCRSSC model on EuroSAT database

Table 3 and Figs. 12 examines the comparison outcomes of the LTCNN-WCRSSC algorithm on the UC Merced dataset with current techniques [25, 26]. The results emphasized that the EfficientNet, MobileNet, ResNet-50, ShuffleNet, TGRRS-DK, and DLB-LULCC models have indicated worse performance. Meanwhile, the RSSC-DBOEDL approach has attained closer results with $accu_y$, $prec_n$, $reca_l$, and $F1_{score}$ of 98.75%, 82.31%, 89.68%, and 78.81% respectively. Besides, the LTCNN-WCRSSC approach indicated better performances with better $accu_y$, $prec_n$, $reca_l$, and $F1_{score}$ of 99.09%, 90.31%, 90.21%, and 90.13% respectively

Table 3: Comparative analysis of the LTCNN-WCRSSC approach on the UC Merced database

UC Merced Dataset				
Method	$\boldsymbol{Accu_y}$	$\boldsymbol{Prec_n}$	$\boldsymbol{Reca_l}$	$\boldsymbol{F1_{score}}$
EfficientNet Method	88.00	88.87	86.25	76.42
MobileNet Model	93.00	87.67	82.07	84.28
ResNet-50 Classifier	95.00	86.31	79.44	78.07
ShuffleNet Model	91.00	78.60	76.36	80.37
TGRRS-DK	89.99	83.74	89.62	87.51
DLB-LULCC	90.25	88.54	80.29	76.86
RSSC-DBOEDL	98.75	82.31	89.68	78.81
LTCNN-WCRSSC	99.09	90.31	90.21	90.13

Doi: https://doi.org/10.54216/JCHCI.090101
Received: October 19, 2024 Revised: December 05, 2024 Accepted: January 10, 2025

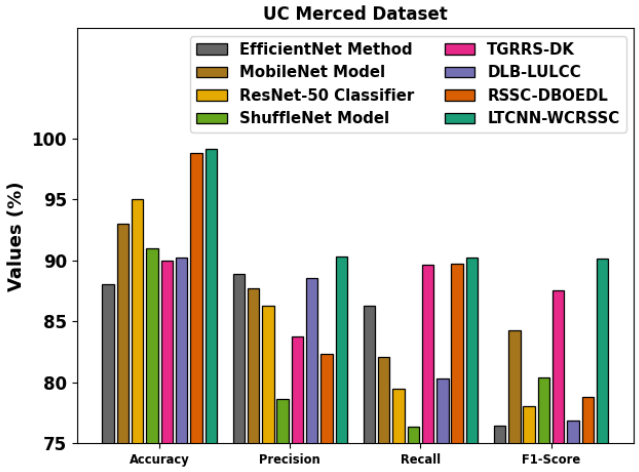

Figure 12: Comparative analysis of LTCNN-WCRSSC model on the UC Merced database

Table 4 and Figs. 13 examine the comparision outcomes of the LTCNN-WCRSSC technique on the EuroSAT dataset with current methods. The results emphasized that the EfficientNet, MobileNet, ResNet-50, ShuffleNet, TGRRS-DK, and DLB-LULCC models have indicated worse performance. Meanwhile, the RSSC-DBOEDL algorithm has obtained closer results with $accu_y$, $prec_n$, $reca_l$, and $F1_{score}$ of 95.07%, 73.18%, 79.2%, and 82.05% correspondingly. Moreover, the LTCNN-WCRSSC system indicated greater performance with high $accu_y$, $prec_n$, $reca_l$, and $F1_{score}$ of 96.67%, 83.28%, 83.09%, and 83.11% correspondingly

Table 4: Comparative analysis of the LTCNN-WCRSSC approach on EuroSAT dataset

EuroSAT Dataset				
Method	$Accu_y$	$Prec_n$	$Reca_l$	$F1_{score}$
EfficientNet Method	85.23	75.52	73.73	82.06
MobileNet Model	87.52	82.19	77.91	81.48
ResNet-50 Classifier	90.34	70.33	71.13	75.05
ShuffleNet Model	88.68	72.63	70.66	77.38
TGRRS-DK	85.12	73.74	82.97	74.68
DLB-LULCC	90.55	74.56	78.55	71.77
RSSC-DBOEDL	95.07	73.18	79.2	82.05
LTCNN-WCRSSC	96.67	83.28	83.09	83.11

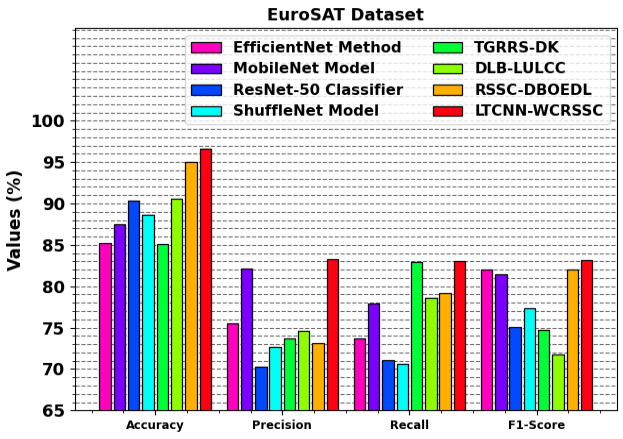

Figure 13: Comparative analysis of the LTCNN-WCRSSC approach on EuroSAT database

Doi: https://doi.org/10.54216/JCHCI.090101
Received: October 19, 2024 Revised: December 05, 2024 Accepted: January 10, 2025

5. Conclusion

In this work, we have designed and developed a LTCNN-WCRSSC algorithm. The LTCNN-WCRSSC technique is designed for efficient RSS classification in resource-constrained devices with on-board training capabilities. To accomplish that, the LTCNN-WCRSSC model contains various phases like feature extraction, image preprocessing, classification model, and hyperparameter tuning method. At first, the LTCNN-WCRSSC model applies image processing using MF to eliminate the noise. Next, the feature extraction process can be exploited by the ConvNeXt-Tiny model. For the RSSC model, the STA-BiLSTM technique is performed. Eventually, the WCA-based hyperparameter selection process can be performed to optimize the classification results of the STA-BiLSTM system. The experimental evaluation of the LTCNN-WCRSSC technique takes place using a benchmark image dataset. The stimulation results indicated the superior performances of the LTCNN-WCRSSC model over other methods.

Data Availability Statement: The data that support the findings of this study are openly available at http://weegee.vision.ucmerced.edu/datasets/landuse.html and https://www.kaggle.com/datasets/apollo2506/eurosat-dataset , reference number [23, 24].

References

[1] Kothandhapani, A. and Vatsal, V., 2020. Methods to leverage onboard autonomy in remote sensing. In *2nd National Conference on Small Satellite Technology and Applications-2020*.

[2] Aposporis, P., 2020, December. Object detection methods for improving UAV autonomy and remote sensing applications. In *2020 IEEE/ACM International Conference on Advances in Social Networks Analysis and Mining (ASONAM)* (pp. 845-853). IEEE.

[3] Yebes, J.J., Montero, D. and Arriola, I., 2020. Learning to automatically catch potholes in worldwide road scene images. *IEEE Intelligent Transportation Systems Magazine*, *13*(3), pp.192-205.

[4] Kyrkou, C. and Theocharides, T., 2020. EmergencyNet: Efficient aerial image classification for drone-based emergency monitoring using atrous convolutional feature fusion. *IEEE Journal of Selected Topics in Applied Earth Observations and Remote Sensing*, *13*, pp.1687-1699.

[5] Naccari, F., Guarneri, I., Curti, S. and Savi, A.A., 2020, November. Embedded Acoustic Scene Classification for Low Power Microcontroller Devices. In *DCASE* (pp. 105-109).

[6] Li, E., Xia, J., Du, P., Lin, C. and Samat, A., 2017. Integrating multilayer features of convolutional neural networks for remote sensing scene classification. *IEEE Transactions on Geoscience and Remote Sensing*, *55*(10), pp.5653-5665.

[7] Sudharsan, B., Breslin, J.G. and Ali, M.I., 2020, October. Edge2train: A framework to train machine learning models (svms) on resource-constrained iot edge devices. In *Proceedings of the 10th International Conference on the Internet of Things* (pp. 1-8).

[8] Hu, F., Xia, G.S., Hu, J. and Zhang, L., 2015. Transferring deep convolutional neural networks for the scene classification of high-resolution remote sensing imagery. *Remote Sensing*, *7*(11), pp.14680-14707.

[9] Yebes, J.J., Montero, D. and Arriola, I., 2020. Learning to automatically catch potholes in worldwide road scene images. *IEEE Intelligent Transportation Systems Magazine*, *13*(3), pp.192-205.

[10] Yu, X., Wu, X., Luo, C. and Ren, P., 2017. Deep learning in remote sensing scene classification: a data augmentation enhanced convolutional neural network framework. *GIScience & Remote Sensing*, *54*(5), pp.741-758.

[11] Wu, J., Fang, L. and Yue, J., 2024. TAKD: Target-Aware Knowledge Distillation for Remote Sensing Scene Classification. *IEEE Transactions on Circuits and Systems for Video Technology*.

[12] Le, T.D., Ha, V.N., Nguyen, T.T., Eappen, G., Thiruvasagam, P., Garces-Socarras, L.M., Chou, H.F., Gonzalez-Rios, J.L., Merlano-Duncan, J.C. and Chatzinotas, S., 2024. On-board Satellite Image Classification for Earth Observation: A Comparative Study of Pre-Trained Vision Transformer Models. *arXiv preprint arXiv:2409.03901*.

[13] Rashid, H.A., Sarkar, A., Gangopadhyay, A., Rahnemoonfar, M. and Mohsenin, T., 2024. TinyVQA: Compact Multimodal Deep Neural Network for Visual Question Answering on Resource-Constrained Devices. *arXiv preprint arXiv:2404.03574*.

[14] Wang, G., Zhang, N., Wang, J., Liu, W., Xie, Y. and Chen, H., 2024. Knowledge distillation-based lightweight change detection in high-resolution remote sensing imagery for on-board processing. *IEEE Journal of Selected Topics in Applied Earth Observations and Remote Sensing*.

[15] Shendy, R. and Nalepa, J., 2024. Few-shot satellite image classification for bringing deep learning on board OPS-SAT. *Expert Systems with Applications*, *251*, p.123984.

[16] Dai, W., Shi, F., Wang, X., Xu, H., Yuan, L. and Wen, X., 2024. A multi-scale dense residual correlation network for remote sensing scene classification. *Scientific Reports*, *14*(1), p.22197.

Doi: https://doi.org/10.54216/JCHCI.090101
Received: October 19, 2024 Revised: December 05, 2024 Accepted: January 10, 2025

[17] Ye, Z., Zhang, Y., Zhang, J., Li, W. and Bai, L., 2024. A multiscale incremental learning network for remote sensing scene classification. *IEEE Transactions on Geoscience and Remote Sensing*.
[18] Liu, X., Wu, W., Hu, Z. and Sun, Y., 2024. SCECNet: self-correction feature enhancement fusion network for remote sensing scene classification. *Earth Science Informatics*, pp.1-19.
[19] Chen, J., Wang, C., Ma, Z., Chen, J., He, D. and Ackland, S., 2018. Remote sensing scene classification based on convolutional neural networks pre-trained using attention-guided sparse filters. *Remote Sensing*, *10*(2), p.290.
[20] Perdana, R.A. and Arimurthy, A.M., 2024. Remote Sensing Scene Classification using ConvNeXt-Tiny Model with Attention Mechanism and Label Smoothing. *Jurnal RESTI (Rekayasa Sistem dan Teknologi Informasi)*, *8*(3), pp.389-400.
[21] Mu, S., Liu, B., Gu, J., Lien, C. and Nadia, N., 2024. Research on Stock Index Prediction Based on the Spatiotemporal Attention BiLSTM Model. *Mathematics*, *12*(18), p.2812.
[22] Das, S.C., Akhtar, F., Alrasheedi, A.F. and Shaikh, A.A., 2024. Application of water cycle algorithm with demand follows green level and nonlinear power pattern of the product for an inventory system. *Scientific Reports*, *14*(1), p.20995.
[23] http://weegee.vision.ucmerced.edu/datasets/landuse.html
[24] https://www.kaggle.com/datasets/apollo2506/eurosat-dataset
[25] Alamgeer, M., Al Mazroa, A., Alotaibi, S.S., Alanazi, M.H., Alonazi, M. and Salama, A.S., 2024. Improving remote sensing scene classification using dung Beetle optimization with enhanced deep learning approach. *Heliyon*, *10*(18).
[26] Ghanbarzadeh, A. and Soleimani, H., 2023. Self-supervised in-domain representation learning for remote sensing image scene classification. *Heliyon*.

Doi: https://doi.org/10.54216/JCHCI.090101
Received: October 19, 2024 Revised: December 05, 2024 Accepted: January 10, 2025